BULLETIN OF THE CHEMICAL SOCIETY OF JAPAN VOL. 39 287—295 (1966)

Fractures in Thin-sectioned Corundum Crystals

By Goro YAMAGUCHI, Yasushi KUBO and Hiroshi OGAWA

Department of Industrial Chemistry, Faculty of Engineering, The University of Tokyo, Hongo, Tokyo

(Received May 26, 1965)

The fracture properties of corundum crystals have been examined on various artificial corundums, such as electrically-fused corundum, Verneuil-flame-fused corundum and hydrothermally-synthetised corundum. The specimens were ground to a tihckness of less than 5/100 mm. The microcracks generated in the grinding process were observed by means of a polarizing microscope. The orientation of the c-axis (C) and the crack normal to the section normal (T) was measured using a universal stage. The direction of the crack has a close relation to the crystal orientation of the thin section. Frequent irregular cracks intercrossing one another occur in crystals ground with T$\wedge$C angles from 0° to 50°. Cleavage cracks along the $\{10\bar{1}1\}$ plane take place prominently in the range of T$\wedge$C angles from 50° to 80°. Rare irregular cracks streaming in one direction take place in the range of T$\wedge$C angles from 80° to 90°. The heat treatment in air of titania-containing corundum decreases the number of cracks in the crystal. The results have been interpreted on the basis of the cohesion strength theory of M. D. Shappel (*Am. Mineralogist,* **21**, 75 (1936)). In order to explain the limited range of the ocurrence of cleavage cracks, a model has been proposed in which the shearing along the cleavage plane takes place prior to the crack nucleation in the corundum crystal.

The fracture properties of corundum are of practical importance as well as of theoretical interest. Its abrasive properties are inferred to depend on the relation between the hardness and the toughness of the corundum.

According to the literature, fabricators of jewel bearings know by experience a certain technique for avoiding breakage loss. The fracture mechanisms in such materials as metals and ductile minerals have been discussed on the basis of the dislocation theory, but discussion of such brittle minerals of a high hardness and strength as corundum has not progressed.

Information has, however, been provided on the fracture properties of artificial corundums observed in thin sections. In a microscopic observation of electric-furnace-fused alumina abrasives, attention was called to the fact that many microcracks, regular or irregular, were generated in corundum crystals lying in various crystallographic

orientations in thin sections. These carcks were found to develop when the crystal was ground to a thickness of below about 5/100 mm. Careful observation of these cracks by quantitative determination revealed a certain law of fracture in thin-sectioned corundum. Various artificial specimens from electrically-fused corundum, Verneuil-flame-fused corundum and hydrothermally-synthesized corundum were observed.

The results will, in this paper, be compared with a model based on the cohesion strength theory of the crystal plane. A mechanism will be proposed which gives an adequate explanation of the discrepancy in the minimum cohesion strength model and which agrees splendidly with the observations.

Experimental

Specimens.—*Regular and White Alumina.*—Most of the specimens employed were commercial 16-mesh grains of electric-furnace-fused alumina abrasives produced by the Carborundum Company, abrasives which contain from 95 to 97% alumina and the impurities shown in Table I. Corundum is the predominating crystalline phase, and impurities are present for the most part as impure minerals, except that only titania is present in corundum in a solid solution, as is shown in the fifth and sixth rows in Table I.

TABLE I. THE IMPURITY COMPOSITION OF THE SPECIMENS

Specimen	SiO_2	Fe_2O_3	TiO_2	
C32	0.51	0.12	2.46	
R41	0.49	0.15	2.49	
C37	0.26	0.04	tr.	
Japanese commercial abrasive	0.86	0.21	2.34	#24 as-received
	0.10	0.10	1.50	#220 treated with Na_2CO_3-K_2CO_3-H_3BO_3 flux

These grains are made up of from one to twenty corundum crystals, euhedral or anhedral, 2 mm. to 1/10 mm. in size. Small amounts of impure minerals are contained in corundum or form the matrix. Titania-containing corundums in the specimens designated as C32 and R41 range in color from brown to pink. The C37 specimen is the one made from Bayer-process white alumina, with few impurities, though it contains some beta alumina.

Heat-treated Titania-containing Abrasive Grains.—Corundum containing titania in a solid solution is known to change color from pink or brown to bluish, and then to opaline, upon the segregation of titania along a certain crystal plane by heat treatment in air. In titania-containing abrasive aluminas, this change in color is accompanied by a marked improvement in the toughness of the grains.

Fracture properties in thin section were observed to change in this process when Japanese commercial 24-mesh grains were used as received and heat-treated in air at 1250°C for 1 hr.; the latter turns bluish with 3.1% weight increase upon oxidation. The impurity compositions of these grains are shown in the fifth and sixth rows in Table I.

Verneuil and Hydrothermally-synthesized Corundum.—The effect of the crystal-growth technique on fracture properties in thin sections was examined using Verneuil corundum and hydrothermally-synthesized corundum which had been grown on the seed of Verneuil corundum.

The Observation of Microcracks in Thin Sections.—Specimens were ground with a 600-mesh SiC abrasive on a motor-driven disk to a thickness of about 5/100 mm., and then refined with boron carbide finer than 600-mesh by manual grinding to about 2/100 mm. Microcracks were generated in this grinding process, as Fig. 1 shows, when the specimens were thinner than 5/100 mm.

The orientation of the c-axis and of the crack normal relative to the section normal was determined by the microscopic method using a universal stage and subsidiarily by the X-ray Laue back-reflection method.

Results

Characteristics of Fractures Related to the Crystallographic Orientation of the Ground Surface.—Figures 1(a), 1(b), 2(a) and 2(b) show thin sections of grains composed of a number of corundum crystals with various crystallographic orientations relative to the section normal. One can see fractures of various kinds exhibited in each of the crystals, depending on their orientations.

The disposition of the c-axis (C) measured on each of crystals with respect to the section normal (T) and the aspect of fracturing are expressed on stereographic projections of Fig. 1(c) and Fig. 2(c).

One can see a definite tendency, in the range of the $T \wedge C$ angle from 0° to 60°, for fracturing to be prominent; from 60° to 80°, it is prominent or medium, while from 80° to 90° there is little fracturing. Smooth crystals with no fractures, such as 2, 3 and 15 in Fig. 1 and 8, 15 and 16 in Fig. 2, have, almost without exception, the c-axis lying in the section plane.

Irregular Cracks.—Two sorts of fractures can be discriminated in Fig. 1(a) and Fig. 2(a); one consists of linear cracks occurring parallel to one another, while the other consists of curved irregular cracks occurring in random directions. The latter is the cleavage crack taking place parallel to a particular crystal plane. In Fig. 1(a) the irregular crack is prominent, while in Fig. 2(a) the cleavage crack is prominent.

Irregular cracks show a definite dependency on the inclination of the c-axis with respect to the section normal. Characteristic irregular cracks intercrossing in three directions, as is shown in Fig. 3, take place in the crystal with the c-axis perpendicular to the section plane ($T \wedge C = 0$). Inclining from this disposition up to the $T \wedge C$ angle of about 60° gives rise to irregular cracks with a tendency to intercross with one another, as Fig.

Fig. 1 (a) Fig. 1 (b) Fig. 1 (c)

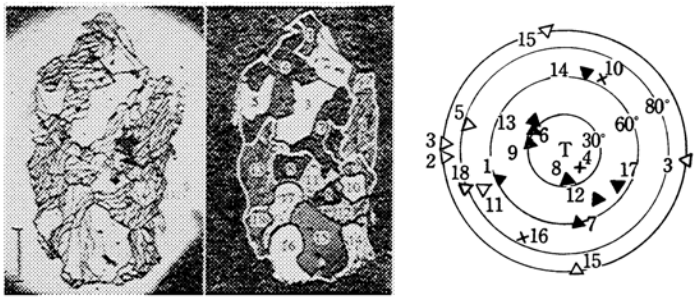

Fig. 1. Aspect of fractures in corundum crystals with various orientations in thin section. Disposition of the c-axis is expressed in (c) by stereographic projection on the section plane where all projections are of the upper intersection, with solid triangles for prominently fractured crystals, open triangles for fractured ones and crosses for medium ones, respectively. Figures affixed to crystals in (b) correspond to ones in (c). ((a) Parallel nicols, (b) Crossed nicols, Specimen R41)

Fig. 2 (a) Fig. 2 (b) Fig. 2 (c)

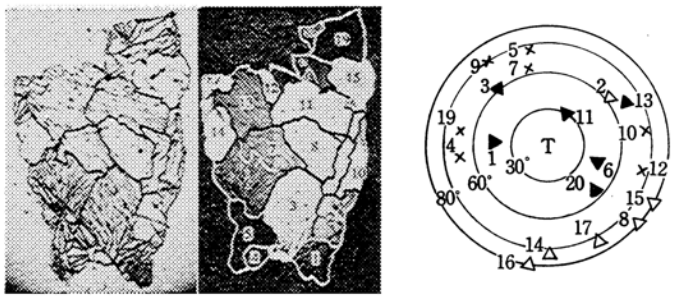

Fig. 2. Aspect of fractures in corundum crystals with various orientations in thin section. Expression is the same as Fig. 1. ((a) Parallel nicols, (b) Crossed nicols, Specimen C32)

Fig. 3 (a) Fig. 3 (b) Fig. 3 (c)

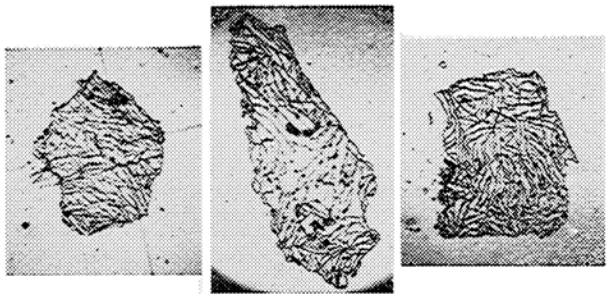

Fig. 3. Fractures in crystals ground perpendicular to the c-axis. (a) Specimen C32, (b) Specimen R41 and (c) Specimen C37

4 shows. The irregular cracks occurring in the region of the T∧C angle between 80° to 90° have a tendency to stream in one direction, as is shown in Fig. 5. In the T∧C range from 50° to 80°, cleavage cracks are the predominating fractures, as will be mentioned in the following section, while at the T∧C angle of 90° no fractures occur.

The dependency on the azimuthal orientation can not be treated separately because of experimental difficulties.

The Cleavage Crack.—The orientation of the c-axis (C) and the cleavage crack normals (P_1, P_2 and P_3, in the order of predominance) with respect to the section normal (T) were determined for crystals in which cleavage cracks take place in different directions in two or three sets. The results for various cases are shown by

Fig. 4. Fig. 5

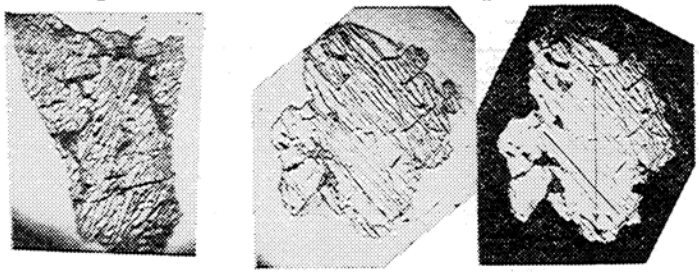

Fig. 4. Fractures in the crystal ground with the angle T∧C less than 60°.
Fig. 5. Fractures in the crystal ground near parallel to the c-axis. (Left; Parallel nicols, Right; Crossed nicols, Specimen C37)

Fig. 6 (a) Fig. 6 (b) Fig. 6 (c)

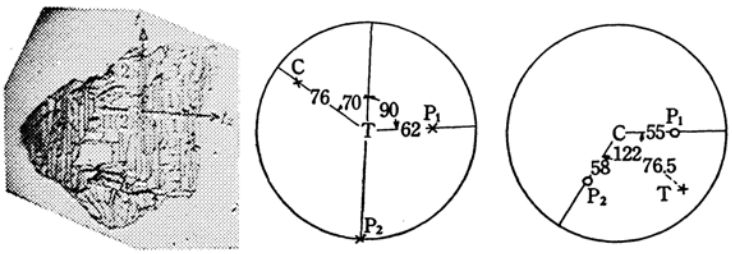

Fig. 6. Orientation of the crystal and the cleavage cracks in thin section of (a) determined by an universal stage and expressed by the stereographic projection (b) on the section plane and (c) on the basal plane. C and T represent the c-axis and the section normal, respectively. P_1, P_2,…… represent the cleavage crack planes less prominent in this order. (Specimen C37)

Fig. 7 (a) Fig. 7 (b) Fig. 7 (c)

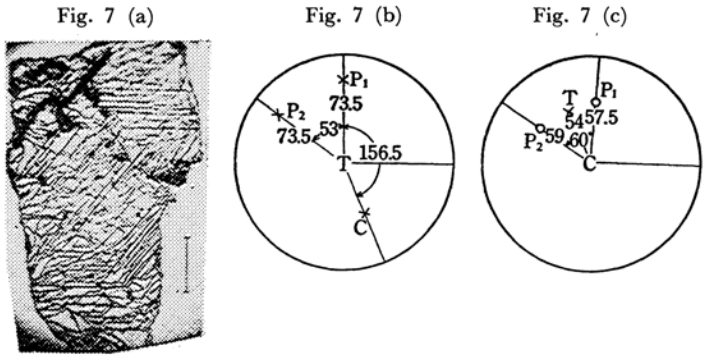

Fig. 7. Orientation of the crystal and the cleavage cracks in thin section. Expression is the same as in Fig. 6. (Specimen R41)

Fig. 8 (a) Fig. 8 (b) Fig. 6 (c)

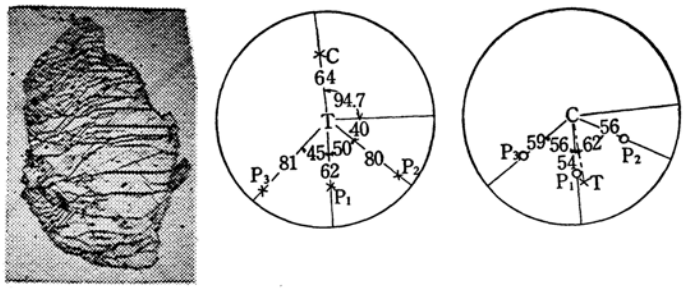

Fig. 8. Orientation of the crystal and the cleavage cracks in thin section. Expression is the same as in Fig. 6. (Specimen C32)

Fig. 9 (a) Fig. 9 (b) Fig. 9 (c)

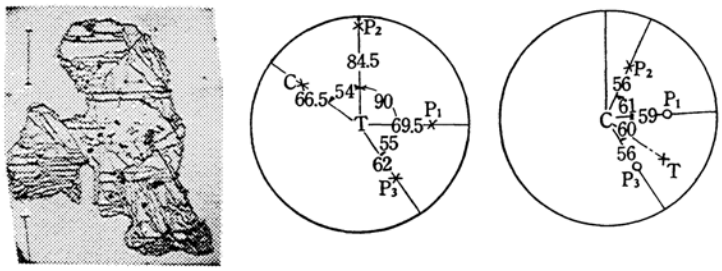

Fig. 9. Orientation of the crystal and the cleavage cracks in thin section. Expression is the same as in Fig. 6. (Specimen R41)

the stereographic projection on the section plane in Fig. 6(b)—9(b), where the orientation corresponds to that of Fig. 6(a)—9(a). These were converted into the stereographic projection on the basal (0001) plane in Fig. 6(c)—9(c) to show the symmetry and the polar angle with respect to the c-axis. The plots by the cross and the open circle represent, as usual, the projection of the upper intersection and the lower intersection respectively. The value of the polar angle measured on a number of crystals is in the 57.5°±5° range, corresponding to that of the rhombohedral $\{10\bar{1}1\}$ plane. The symmetry of the cleavage crack patterns, however, can be interpreted as trigonal or hexagonal for Fig. 6(c), but only as hexagonal for Fig. 7(c)—9(c). This incompatibility may be considered to be due to the formation of basal twinning in electric-furnace-fused corundum.

The conditions for the generation of the cleavage crack were examined, on all of the crystals exhibiting the cleavage crack in a section containing about

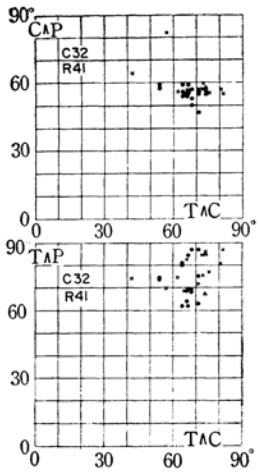

Fig. 10. Condition for generation of the cleavage crack expressed by the angles T∧C, T∧P and C∧P. solid circles represent cleavage cracks with hexagonal arrangement due to basal twinning, solid triangles ones with trigonal and crosses ones with single, respectively. (Specimen C32, R41)

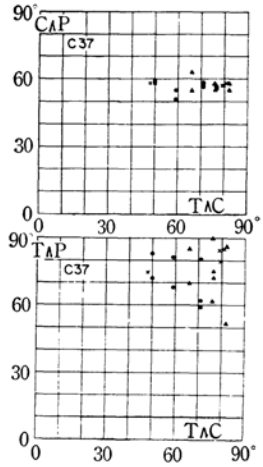

Fig. 11. Condition for generation of the cleavage crack. Expression is the same as in Fig. 10. (Specimen C37)

eighty grains, for the C32, R41(titania-containing) and C37(white alumina) specimens by measuring the T∧C, T∧P and C∧P angles. The results are plotted in Figs. 10 and 11, with solid circles for the hexagonal cleavage, solid triangles for the apparent trigonal cleavage, and crosses for the single cleavage.

It is clear that almost all of the cleavage cracks occur when the crystal is ground with a T∧C angle between 50° and 80° and with a T∧P angle between 60° and 90°.

The Effect of the Heat Treatment on the Fracture Properties of Titania-containing Corundum.—Fig. 12(a) shows the thin sections of corundum crystals as received, containing titania in a solid solution and colored a pale brown. Figure 12(b) shows that of crystals treated in air at 1250°C for 1 hr.; they turned bluish.

A remarkable change in fracture properties is observed when specimens are heat-treated. In the heat-treated specimen, the cleavage crack comes not to take place, but large cracks dividing the crystal into relatively small numbers of blocks appear characteristically.

Fig. 12 (a)

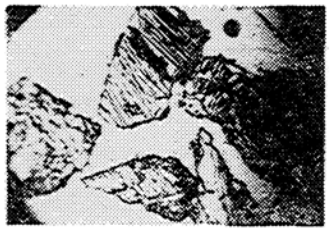

Fig. 12 (b)

Fig. 12. Change of fracture property of titania-containing corundums by heat treatment, (a) as-received and (b) heat treated in air at 1250°C for 1hr to bluish.

Fractures in Verneuil Corundum and Hydrothermal Corundum.—Figure 13 shows a microphotograph with crossed nicols of a thin section of Verneuil corundum on the left of the dividing line, and one of hydrothermal corundum on the right, which has been grown on the seed of the Verneuil corundum with the same crystallographic orientation. Basal fractures are striking in the hydrothermal corundum: they occur in the contact region along the stripes with a high birefringence, but they are interrupted at some distance from the boundary. This region of high birefringence has been shown by an electron probe microanalyzer to be twice as rich in iron content introduced from an autoclave as other regions of the hydrothermal corundum. Outside the contact region of the hydrothermal corundum and in the Verneuil corundum, the cleavage cracks along $r\{10\bar{1}1\}$ take place as usual. The crystal has an orientation with a T∧C angle of 81° and a T∧P angle of 77°.

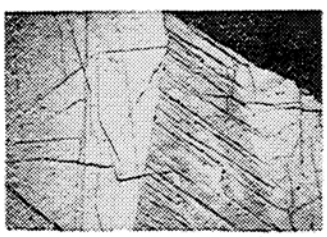

Fig. 13. Fractures in Verneuil corundum and in hydrothermal corundum. Hydrothermal corundum on the right was grown on the seed of Verneuil corundum on the left with the same crystallographic orientation. Stripes in hydrothermal corundum are regions with high birefringence. The crystal was ground with the angle T∧C of 81° and T∧P of 77°. The trace of $r\{10\bar{1}1\}$ and $c\{0001\}$ is shown in the figure. (Crossed nicols)

Discussion

Regarding fracture properties, corundim is known[1] to show no cleavages but two possible partings, one parallel to the basal {0001} plane, and the other parallel to the rhombohedral $\{10\bar{1}1\}$ plane, which is often characterized by the appearance of twin laminations along the same plane. This description is based on a study by Judd[2] which demonstrated that the supposed cleavages in corundum are due to alteration along definite planes of the crystal. When alteration does not exist, the natural corundum is quite destitute of any trace of cleavage, but is usually breaking with an irregular or conchoidal fracture as in quartz; however, a tendency to break up along certain planes, such as $c\{0001\}$, $r\{10\bar{1}1\}$ and $m\{10\bar{1}0\}$, is the result of the incipient alteration, which gives rise to corroded cavities along these planes.

This is obviously incorrect in the case of artificial corundum, such as the electrically-fused, the flame-fused or the hydrothermally-synthesized corundum, which exhibits well-defined cleavages along $r\{10\bar{1}1\}$ in thin sections, as has been shown above.

The fracture properties of materials are usually determined on a relatively large rod, as in loading tests. In such tests corundum exhibits rather conchoidal fractures which bear no clear relation to its crystal structure or to the inherent structural weakness. In thin sections, however, where the bulk strength is extremely reduced, fractures characterized by the structure become predominant. This means that the type of fracture depends on the way it is produced. Therefore, such discussion of corundum as concerns cleavage, parting and conchoidal fracture is meaningless unless the testing method is clearly described.

The cohesion strength of the crystal plane in thin sections has been estimated on corundum and compared with the results obtained above. Using Shappel's cleavability,[3] $V_{|hkl|}$ is defined as:

$$V_{|hkl|} = \frac{A_{|hkl|}}{\sum_i n_i f_i \cos\theta_i}$$

where f_i is the bond strength between a pair of the ions with the cleavage face interpose between them; θ_i, the angle between the bond and the normal of the crystal plane; n_i, the number of such bonds for the ith ion, and $A_{|hkl|}$, the area element

1) J. D. Dana and E. S. Dana, "The System of Mineralogy," 7th ed., Vol. 1, John Wiley & Sons, Inc., New York (1944), p. 520.
2) J. W. Judd, *Min. Mag.*, **11**, 49 (1895).
3) M. D. Shappel, *Am. Mineralogist*, **21**, 75 (1936).

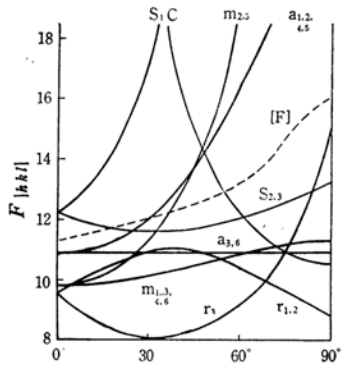

$\Phi = -30°$ T∧C

Fig. 14 (a)

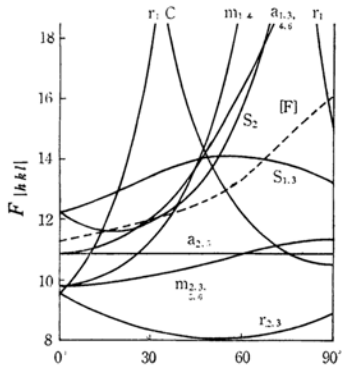

$\Phi = 30°$ T∧C

Fig. 14 (b)

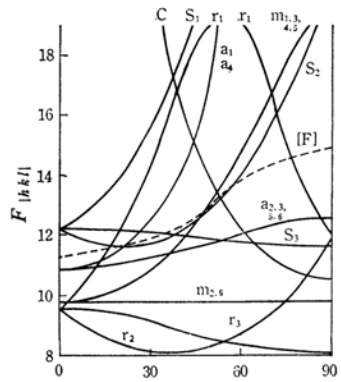

$\Phi = 0°, (60°)$ T∧C

Fig. 14 (c)

Fig. 14. Dependence of the cohesion strength of crystal plane in thin scetion, $F_{|hkl|}$, on the polar grinding direction on main zones, T∧C.

of the crystal plane. The estimated cohesion strength, $F_{|hkl|}$, of the crystal plane in thin sections is derived as:

$$F_{|hkl|} = \frac{\mathrm{cosec}(\mathrm{T}\wedge\mathrm{P})}{V_{|hkl|}}$$

where T∧P is the angle between the section normal and the normal of the crystal plane and where cosec(T∧P) represents the cross area of the crystal plane in thin sections. The value of the cleavability, $V_{|hkl|}$, of corundum was calculated by Shappel to be as given in the seventh column of Table II, where the bond strength, f_i, is estimated from the coordination theory of ionic structures.

The value of the cohesion strength, $F_{|hkl|}$, at different T∧C angles along main zones has been calculated for each of the crystal planes, as is given in Fig. 14. The crystallographic data on main crystal planes of corundum are shown in Table II and Fig. 15.

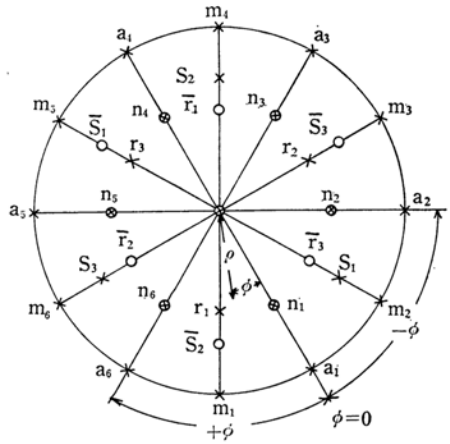

Fig. 15. Stereographic projection showing main crystal planes of corundum and designation in this paper.

In the range of T∧C angles larger than about 20°, the cohesion strength of $r\{10\bar{1}1\}$ becomes conspicuously lower than in other ranges. The basal (0001) plane can not be a cleavage plane; this conclusion, based on the cohesion strength calculation, is in conformity with the fact that the basal fracture in hydrothermally-synthesized corundum, in the contact region with the seed, may be referred to as the parting which is produced by the zonal segregation of the impurity iron along the same plane.

For the crack in the thin section with the T∧C angle of 0°, a possible interpretation is that the main direction of the irregular cracks are parallel to the $m\{10\bar{1}0\}$; the crack faces are nearly perpendicular to the section plane, and the small differences in cohesion strength among the crystal planes in this orientation cause an irregular deviation in the crack direction.

In order to estimate the strength of corundum at various crystallographic orientations of the ground surface, we will define the strength factor, [F], as:

TABLE II. CRYSTALLOGRAPHIC DATA ON MAIN CRYSTAL PLANES OF CORUNDUM

Form	Index: Morphological rhombohedral	Index: Hexagonal (adopted in this paper)	Index: Structural hexagonal	σ in Fig. 15	Φ in Fig. 15	Shappel's cleavability
c	111	0001	0001	0°00′	—	9.5
m	$2\bar{1}\bar{1}$	$10\bar{1}0$	$01\bar{1}0$	90°00′	30°00′	10.2
a	$10\bar{1}$	$11\bar{2}0$	$11\bar{2}0$	90°00′	0°00′	9.2
r	100	$10\bar{1}1$	$01\bar{1}2$	57°35′	30°00′	12.4
s	$11\bar{1}$	$02\bar{2}1$	$10\bar{1}1$	72°23′	−30°00′	8.6
n	$31\bar{1}$	$22\bar{4}3$	$11\bar{2}3$	61°11½′	0°00′	

$$\frac{1}{[F]} = \frac{1}{n}\sum_{i=1}^{n}\left(\frac{1}{F_i}\right)$$

where F_i corresponds to $F_{|hkl|}$ and where $[F]$ is shown approximately as follows:

$$\frac{1}{[F]} = \frac{1}{13}\left(\frac{1}{F_{a_1}}+\frac{1}{F_{a_2}}+\frac{1}{F_{a_3}}+\frac{1}{F_{s_1}}+\frac{1}{F_{s_2}}+\frac{1}{F_{s_3}}+\frac{1}{F_{m_1}}+\frac{1}{F_{m_2}}+\frac{1}{F_{m_3}}+\frac{1}{F_c}+\frac{1}{F_{r_1}}+\frac{1}{F_{r_2}}+\frac{1}{F_{r_3}}\right)$$

We may expect qualitatively that the increase of $[F]$ will correspond to the decrease in fracturing. The calculated values in each azimuthal direction (ϕ) are shown by dotted lines in Fig. 14. From this we can see that $[F]$ increase as the T∧C angle increases from 0° to 90°, regardless of the azimuthal direction; this finding coincides with the observation that fracturing decreases as the T∧C angle increases from 0° to 90°.

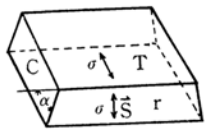

Fig. 16. Schematic representation of each planes, T the surface plane, c the basal plane and r the cleavage plane. Cleavage cracks take place only in the range of the angle T∧C from 50° to 80°. α represents the angle T∧C.

The limited range of the occurrence of cleavage cracks might have the significance explained below, in view of the crystal structure of corundum. Figure 17 illustrates the packing of ions parallel to the $\{10\bar{1}1\}$ plane. On the cleavage surface, there exist the directions shown by the arrows designated $\vec{S}$, with the angle of 18° from the trace of the basal (0001) plane and with the T∧C angle of 75°, which corresponds to the direction leading to a saddle point, and the other direction shown by the arrows $\vec{R}$ with the angle of 29° from the trace of the basal (0001) plane and with the T∧C angle

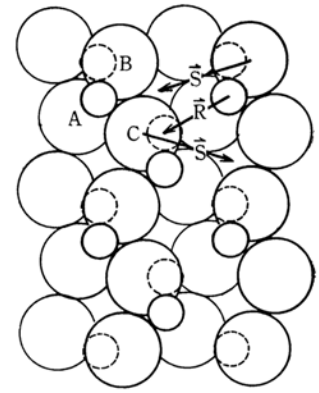

Fig. 17 (a)

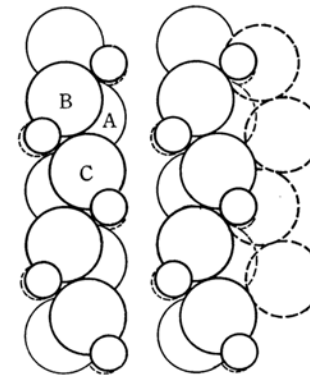

Fig. 17 (b)

Fig. 17. Packing of ions normal to $\{10\bar{1}1\}$. Two layers of ions on both sides of cleavage surface are shown in (a), and arrangement after the shear $\vec{R}$ is shown in (b).

of 66°, which corresponds to the direction in which the Al ions on the upper layer may be transported to just above the Al ions on the lower layer. Most of the plots fall in the T∧C regions between 66° and 75°. If a shear is applied between these two layers, a great resistance may be anticipated in directions other than the adjacent region of the $\vec{S}$ direction. When the shear shown by the $\vec{R}$ vector is applied, it gives rise to the arrangement of ions on both sides of the cleavage surface shown

in Fig. 17, where no bonding exists between the two crystal faces, and where only repulsions work between anions and between cations. Therefore, the experimental results have been interpreted as suggesting a fracture mechanism in which a shear along the cleavage face is required prior to the cleavage-crack nucleation.

The change in fracture properties upon heat treatment on titania-containing corundum may be interpreted on the assumption of this mechanism that the exsolution of the titania[4] nuclei in the corundum makes the shear quite difficult by nailing up the crystal plane.

Conclusion

1) When corundum crystals are ground in thin sections below the thickness of about 5/100 mm., fractures characterized by the inherent structure occur in the grinding process. The previous descriptions of the fracture properties of corundum are not sufficient in that they neglect the dependence of the type of fracture on the testing method.

2) These microcracks have a close relation to the section direction with respect to the crystal orientation. Irregular cracks with a tendency to intercross with one another occur frequently in crystals ground with T∧C angles from 0° to 50°. Cleavage cracks along the $r\{10\bar{1}1\}$ plane take place prominently in the range of the T∧C angles from 50° to 80°. Irregular cracks with a tendency to stream in one direction occur rarely in the range from 80° to 90°.

3) The results have been interpreted in terms of the cohesion strength of the crystal plane calculated on the basis of the ionic-bonding-strength theory. In order to explain the limited range of the occurrence of cleavage cracks, a model based on the shearing along the cleavage face prior to the crack nucleation has been proposed.

4) Heat treatment in air on titania-containing corundum has a conspicuous effect on the fracture properties.

5) Verneuil corundum and hydrothermal corundum exhibit no conspicuous differences in fracture properties, and the basal parting in the contact region of hydrothermal corundum on a seed is due to the zonal segregation of the iron impurity.

4) T. Horibe and S. Kuwabara, *J. Chem. Soc. Japan, Ind. Chem. Sect.* (*Kogyo Kagaku Zasshi*), **67**, 2033 (1964).